Original Article

Visualisation of multiple organ amyloid involvement in systemic amyloidosis using ^{11}C-PiB-PET imaging

Naoki Ezawa[1], Nagaaki Katoh[1], Kazuhiro Oguchi[2], Tsuneaki Yoshinaga[1], Masahide Yazaki[3,4] and Yoshiki Sekijima[1,2,4]

[1]Department of Neurology and Rheumatology, Shinshu University School of Medicine, 3-1-1 Asahi, Matsumoto, Japan

[2]Jisenkai Brain Imaging Research Center, 2-5-1 Honjyo, Matsumoto, Japan

[3]Department of Biomedical Laboratory Sciences, Shinshu University School of Health Sciences, 3-1-1 Asahi, Matsumoto, Japan

[4]Institute for Biomedical Sciences, Shinshu University, 3-1-1 Asahi, Matsumoto, Japan

Correspondence to: Nagaaki Katoh, Department of Medicine (Neurology and Rheumatology), Shinshu University School of Medicine, 3-1-1 Asahi, Matsumoto, Nagano 390-8621, Japan

E-mail: nagaaki@shinshu-u.ac.jp

Tel: +81-263-37-2673, Fax: +81-37-3427

ORCID ID: 0000-0002-6993-0607

Abstract

Purpose: To investigate the utility of the Pittsburgh compound B (PiB) positron emission tomography (PET) imaging technique for evaluating whole-body amyloid involvement in patients with systemic amyloidosis.

Methods: Whole-body ^{11}C-PiB-PET was performed in seven patients with systemic immunoglobulin light-chain (AL) amyloidosis, seven patients with hereditary transthyretin (ATTRm) amyloidosis, one asymptomatic *TTR* mutation carrier and three healthy controls. The correlations between clinical organ involvement, radiological ^{11}C-PiB uptake and histopathological findings were analysed in each organ.

Results: ^{11}C-PiB-PET imaging showed good correlations between clinical and radiological organ involvement in the heart and stomach. Abnormal tracer uptake was also observed in the spleen, lachrymal gland, submandibular gland, sublingual gland, lymph node, brain, scalp, extraocular muscles, nasal mucosa, pharynx, tongue and nuchal muscles, most of which were asymptomatic. Physiological tracer uptake was universally observed in the urinary tract (kidney, pelvis, ureter and bladder) and enterohepatic circulatory system (liver, gallbladder, bile duct and small intestine) in all participants. Most of the patients and one healthy control subject showed asymptomatic tracer uptake in the lung and parotid gland. The peripheral nervous system did not show any tracer uptake even in patients with apparent peripheral neuropathy. Histological amyloid deposition was confirmed in biopsied myocardium and gastric mucosa where abnormal ^{11}C-PiB retention was observed.

Conclusions: ^{11}C-PiB-PET imaging can be clinically utilised in systemic evaluation of amyloid distribution in AL and ATTRm amyloidosis patients. Quantitative analysis of

^{11}C-PiB-PET is expected to be useful in therapy evaluation and will reveal whether amyloid clearance is correlated with clinical response.

Key words: amyloid, Pittsburgh compound B -PET, amyloid imaging, light-chain amyloidosis, hereditary transthyretin amyloidosis

Introduction

Systemic amyloidosis is a group of diseases associated with progressive deposition of circulating amyloid precursor protein in a number of vital organs, which eventually results in fatal multiple organ dysfunction unless properly treated. Appropriate diagnosis and treatment at the early stage are therefore critically important to improve prognosis. To develop an adequate treatment plan, it is essential to confirm amyloid deposition and to evaluate the extent of organ involvement. At present, histopathological examination of biopsied tissue specimens is performed to confirm amyloid deposition. However, this has a number of limitations, including relatively high invasiveness and the requirement for specific operator skills. In addition, tissue biopsy can be used to evaluate amyloid deposition only in a limited area of a single organ. Therefore, whole-body amyloid imaging is becoming to be a novel, useful, and less invasive method to evaluate systemic amyloidosis.

Carbon-11-labelled Pittsburgh compound B (^{11}C-PiB; 2-[4'-methylaminophenyl]-6-hydroxybenzothiazole)-positron emission tomography (PET) is an established amyloid imaging technique used to evaluate localised Aβ amyloid deposition in the brains of patients with Alzheimer's disease [1] and Aβ-type cerebral amyloid angiopathy [2]. PiB is a derivative of the amyloid-binding dye, thioflavin-T [3], and it can therefore theoretically combine with various amyloid proteins. Recent studies indicated that PiB is capable of detecting other types of amyloidosis [4-6]. Here, we investigated the feasibility of using ^{11}C-PiB-PET for evaluating whole-body amyloid deposition in two major types of systemic amyloidoses, i.e., systemic immunoglobulin light-chain (AL) and hereditary transthyretin (ATTRm) amyloidosis.

Material and methods

Participants

The clinical information of participants is summarised in Table 1. From June 2015 to December 2016, histologically proven systemic AL amyloidosis patients (n = 7; mean age ± SD, 63.7 ± 10.6; range 52–82), histologically and genetically proven ATTRm amyloidosis patients (n = 7; mean age ± SD, 44.3 ± 11.3; range 23 – 58), asymptomatic *TTR* gene mutation carrier (n = 1; 28 years old) and healthy control volunteers (n = 3; mean age ± SD, 42.3 ± 6.7; range 38 – 50) were enrolled in this study. All patients were diagnosed and examined at Shinshu University Hospital. All of the AL amyloidosis patients were newly diagnosed untreated patients with the exception of one patient (patient 1, Table 1) who received chemotherapy but relapsed before achieving any clinical organ response. The *TTR* genotypes of ATTRm amyloidosis patients were as follows: V30M (p.V50M) heterozygous, n = 5; G47R (*p*.G67R) heterozygous, n = 1; T60A (p.T80A) heterozygous, n = 1. All except one ATTRm patients (patient 14) received anti-amyloid therapies, liver transplantation and/or tafamidis administration (Table 1). The *TTR* genotype of the asymptomatic mutation carrier (patient 15, Table 1) was D18G (p.D38G).

Clinical evaluation

Clinical organ involvements due to systemic amyloid deposition were evaluated in all participants at the time of the scan. The international consensus guidelines from the 10th International Symposium on Amyloidosis [7] were used to determine organ involvement of

the heart, kidney, liver, gastrointestinal tract, lung, sensorimotor and autonomic nervous system, tongue and lymph nodes (Table 2). Reduced gastric motility was demonstrated gastroendoscopically by confirming residual gastric contents ingested on the day before gastroendoscopy. These criteria were originally designed for evaluating AL amyloidosis. However, we used these criteria for evaluating both AL and ATTRm amyloidosis in this study as no established evaluation method was available for ATTRm amyloidosis. With regard to other organs without consensus involvement criteria, organ-related symptoms were simply described, but possible correlations between symptoms and amyloid involvement are not discussed.

^{11}C-PiB-PET imaging

All imaging was performed with a PET/CT scanner (Discovery PET/CT 600; GE Healthcare, Milwaukee, WI). Thirty minutes after administration of 500-636 MBq of ^{11}C-PiB, whole-body low-dose CT covering the vertex to the pelvis was performed. After CT scan, seven bed positions emission scans were followed by a 2-minutes per bed scan in 3D mode. The images were reviewed by trained amyloidologists and radiologist among the authors (N.E, N.K, K.O and Y.S). Both maximum intensity projection (MIP) images (Fig. 1) and transaxial images (Fig. 2) were visually investigated in the conventional manner to evaluate positive tracer uptake in the body. For brain evaluation, standardised uptake value ratio (SUVR) images (Fig. 2Aa, Ba, Ca) were generated by normalising ^{11}C-PiB uptake relative to pontine uptake [2], because ^{11}C-PiB uptake in the brain was weaker than those in other involved organs in the body (Figs. 1 and 2) and abnormal ^{11}C-PiB retention was observed in

the cerebellum but not in the pons in ATTRm amyloidosis patients [6]. In this study, only the leptomeningeal type brain uptake [6] but not Alzheimer's disease type was taken as significantly positive brain uptake because we intended to evaluate the amyloid deposition derived from systemic amyloidosis but not from localised Aβ amyloidosis. With regard to the scalp, the tracer uptake was determined as significantly positive only when tracer uptake was stronger than that of the brain white matter in SUVR images (Fig. 2Ca). These abnormal tracer uptake intensities were graded on a visual rating scale as follows: +, mild; ++, moderate; and +++, intense uptake (Table 1).

Histopathological analysis

The correlations between histopathological findings of biopsied specimens and ^{11}C-PiB-PET findings were investigated retrospectively to validate the feasibility of ^{11}C-PiB-PET. Histopathological analysis, including Congo red staining and immunohistochemical staining, was performed as described previously [8].

Protocol approval and patient consent

All procedures in studies involving human participants were performed in accordance with the ethical standards of the institutional and/or national research committee and with the 1964 Declaration of Helsinki and its later amendments or comparable ethical standards. This study protocol was approved by the Ethical Committee of Shinshu University School of Medicine and written informed consent was obtained from each participant.

Results

Correlations between clinical manifestations and ^{11}C-PiB-PET images

The clinical background of the participants, organ involvement, and ^{11}C-PiB tracer uptake in each organ are summarised in Table 1. Universal tracer uptake was observed in the urinary tract (kidney, pelvis, ureter and bladder) and enterohepatic circulatory system (liver, gallbladder, bile duct and small intestine) in all participants, including healthy controls (Figs. 1 and 2) due to physiological clearance of ^{11}C-PiB through the renal and hepatobiliary systems [9]. In addition, most of the systemic amyloidosis patients and one healthy control subject showed increased ^{11}C-PiB retention in the lung (Fig. 2Ah, Bh, Ch). This was probably due to reduced pulmonary blood flow and partial volume effect induced by collapsed lung. For these reasons, we excluded the urinary tract, enterohepatic circulatory system and lung from the evaluations.

Common findings for both AL and ATTR amyloidosis

Among the organs evaluated, good correlations between clinical and radiological organ involvement were observed in the heart (Fig. 2Bh, Ch) and stomach (Fig. 2Bi, Ci) in both AL and ATTRm amyloidosis. As shown in Table 1, 11 of 12 patients with clinical cardiac involvement (mean left ventricular wall thickness > 12 mm) showed positive tracer uptake in the heart. The only exception was a 23-year-old female ATTRm patient with G47R mutation (patient 10, Table 1) that did not show increased ^{11}C-PiB retention, although she presented mild cardiac wall thickening (mean left ventricular wall thickness, 14.5 mm), compatible with amyloid cardiomyopathy. Similarly, all of eight patients with clinical gastric involvement

(decreased gastric motility) showed positive gastric ^{11}C-PiB uptake. In addition, two patients (1 AL and 1 ATTRm) showed increased ^{11}C-PiB retention in the gastric wall although they did not have clinical gastric involvement. Radiological involvement was more sensitive than clinical organ involvement in the tongue, as 13 patients (AL, *n* = 6; ATTRm, *n* = 7) showed increased ^{11}C-PiB retention in the tongue (Fig. 1e and f, 2Be and Ce) and two (AL, *n* = 2) had obvious macroglossia (Table 1).

It is likely that ^{11}C-PiB-PET is able to detect subclinical amyloid deposition in the glandular tissues. The salivary glands (parotid gland, submandibular gland and sublingual gland) were the most prominent organs positive for ^{11}C-PiB, and increased retention was observed in four AL and six ATTRm patients. Among them, the submandibular gland was palpable in one AL patient. The amount of ^{11}C-PiB accumulation in salivary glands in ATTRm (Fig. 2Cd – f) was greater than that in AL patients (Fig. 2Bd – f). One healthy control subject showed ^{11}C-PiB retention in the parotid gland, but the level was much lower than those in systemic amyloidosis patients. Eight patients (AL, *n* = 3; ATTRm, *n* = 5) showed increased ^{11}C-PiB retention in the thyroid (Fig. 2Bg, Cg), and five of these patients (AL, *n* = 3; ATTRm, *n* = 2) had subclinical hypothyroidism (Table 1). Six patients (AL, *n* = 4; and ATTRm, *n* = 2; Fig. 2Bi) showed positive ^{11}C-PiB accumulation in the spleen, but none of the patients showed clinical symptoms regarding this organ.

In contrast to other organs, amyloid deposition in the peripheral nervous system was difficult to detect by ^{11}C-PiB-PET. In fact, no patients showed increased ^{11}C-PiB retention in the peripheral nervous system (i.e., nerve root, plexus and peripheral nerves), although six ATTRm patients and one AL patient showed clinically obvious sensorimotor and autonomic

polyneuropathy.

Specific findings for AL amyloidosis

Characteristic abnormal ^{11}C-PiB accumulation in nuchal muscles (Fig. 1b and e, 2Bc – g) was observed only in AL amyloidosis (n = 5), and one of these patients showed dropped head due to weakness of nuchal muscles. Lymph node (n = 1) and extraocular muscles (n = 2; Fig. 1e, 2Bc) were the other organs in which positive ^{11}C-PiB uptake was observed in only AL amyloidosis patients, and none of these patients showed clinical symptoms regarding these organs.

Specific findings for ATTRm amyloidosis

Abnormal ^{11}C-PiB retention in the lachrymal gland (n = 5; Fig. 2Cc), brain (n = 2; Fig. 2Ca), scalp (n = 3; Fig. 2Ca), nasal mucosa (n = 3; Fig. 1f, 2Cd), and pharynx (n = 4; Fig. 2Cd – f) were observed only in ATTRm amyloidosis patients (Table 1). None of the patients showed clinical symptoms regarding these organs, with the exception of one patient with positive lachrymal gland uptake who showed dry eye.

Correlation between ^{11}C-PiB-PET images and histopathological findings

To validate the feasibility of whole-body ^{11}C-PiB-PET to detect amyloid deposition, we investigated the correlation between ^{11}C-PiB-PET images and histopathological findings of biopsied tissues. In this study, gastric mucosal biopsy specimens were available for 10 patients (AL, n = 3; ATTRm, n = 7) and an endomyocardial biopsy specimen was available in

one ATTRm patient. Considerable amyloid deposition was observed in muscularis mucosae and submucosal connective tissue in all gastric mucosal biopsy specimens and abnormal ^{11}C-PiB retention in the gastric wall was observed in each patient (Fig. 3a – d). Endomyocardial biopsy was performed in a 58-year-old male ATTRm patient (patient 14, Table 1) with a 2-year history of cardiac dysfunction. Histopathological examination demonstrated moderate ATTR amyloid deposition in the cardiac interstitium and ^{11}C-PiB-PET showed abnormal tracer retention in the cardiac wall, compatible with the histopathological findings (Fig. 3e – h).

Discussion

Several previous studies investigated the utility of whole-body molecular imaging to visualise systemic amyloid deposition using various tracers (Table 3) [10-28]. Serum amyloid P component labelled with iodine-123 (^{123}I-SAP) scintigraphy is the most intensively investigated diagnostic test for whole-body amyloid imaging, and can detect amyloid deposition in several types of systemic amyloidosis, including AL, ATTRm, Aβ2M and AApoAI amyloidosis [10-13]. However, ^{123}I-SAP scintigraphy cannot sufficiently evaluate amyloid deposition in the heart [10, 11, 13], which is the most important organ in systemic amyloidosis patients to determine prognosis and treatment management. In addition, the availability of ^{123}I-SAP is limited to certain specialised institutions [29].

Bone-seeking tracers, including ^{99m}Tc-3,3-diphosphono-1,2-propanodicarboxylic acid (DPD), ^{99m}Tc-pyrophosphate (PYP) and ^{99m}Tc-methylene diphosphonate (MDP), have also been reported to be useful for detecting systemic amyloidosis in ATTRm, wild-type ATTR

(ATTRwt), AL and AApoAI amyloidosis [30]. Notably, bone-seeking tracers are very sensitive to detect cardiac ATTR amyloidosis [19, 20]. However, these tracers are unable to detect cardiac amyloid involvement in AL amyloidosis [14, 17, 18]. In addition, bone-seeking tracers are not useful to detect amyloid deposition in most visceral organs other than the heart [14-18] (Table 3).

Recently, two fluorine-18 (^{18}F)-labeled tracers, ^{18}F-florbetapir [21-25] and ^{18}F-florbetaben [26], were reported to be potential whole-body amyloid imaging molecules. Although ^{18}F-florbetapir-PET was shown to be able to detect cardiac involvement in patients with AL and ATTR amyloidosis [21], the data concerning its ability to detect amyloid involvement of the other organs are limited to case reports [23-25] (Table 3). Further experience in using this tracer for systemic amyloid evaluation in larger cohorts is needed. With regard to ^{18}F-florbetaben, only one case report showed positive uptake of the tracer in several organs in a patient with AL amyloidosis [26]. Further investigation of the correlation between ^{18}F-florbetaben uptake and histopathological findings in a group study setting is required. ^{99m}Tc-Aprotinin [27, 28] was reported to show a similar uptake pattern to ^{11}C-PiB in AL amyloidosis patients (Table 3). However, its usability in evaluating ATTR amyloidosis is unclear due to the small number of patients investigated [27, 28], and this tracer is no longer used widely because of the withdrawal of bovine aprotinin from the market [22].

The greatest advantage of ^{11}C-PiB-PET demonstrated in this study was that this widely available tracer can detect cardiac amyloid deposition very clearly in AL amyloidosis patients as well as in ATTRm amyloidosis patients. In addition, ^{11}C-PiB-PET visualised AL and ATTRm amyloid deposition in other organs, including the stomach, spleen, lymph nodes,

brain, glandular tissues and soft tissues. In particular, it is notable that there was a good correlation between clinical and radiological involvement in the stomach in both AL and ATTRm amyloidosis patients (Table 1). To our knowledge, there have been no reports of other tracers that can detect amyloid deposition in the gastric wall.

In this study, we confirmed the correlations between ^{11}C-PiB-PET images and histopathological findings in the stomach and heart (Fig. 3). In addition, we recently showed that ^{11}C-PiB-PET could detect leptomeningeal ATTR amyloid deposition with high sensitivity [6]. Other organs, including the spleen [31], lachrymal glands [32], salivary glands [33, 34], thyroid [35] and lymph nodes [36], have been reported to be histologically involved in patients with systemic amyloidosis. In this study, histological confirmation of amyloid deposition was not obtained from these organs but they were positively delineated by ^{11}C-PiB-PET only in patients with systemic amyloidosis, but not in asymptomatic *TTR* mutation carriers or healthy controls. Therefore, increased ^{11}C-PiB retention in these organs was considered to delineate amyloid deposition, and histological amyloid deposition in these organs may be more common than previously thought. However, detailed histology (biopsy and/or autopsy)-based studies will be required to confirm the relationship between radiological tracer uptake intensity and histological amyloid burden in each organ.

This study identified several limitations of ^{11}C-PiB-PET for clinical use in evaluating systemic amyloidosis. The first is its lack of ability to assess the amyloid involvement in the urinary tract and enterohepatic circulatory system due to the physiological clearance pathway of PiB through the renal and hepatobiliary systems. This nature of ^{11}C-PiB-PET could be a major limitation when evaluating patients with systemic AL amyloidosis, as both the kidney

and liver are commonly involved in this disease [37, 38]. It was also shown that ^{11}C-PiB-PET was unable to distinguish the pathological lung uptake from physiological uptake, as not only amyloidosis patients but also one healthy control subject showed increased ^{11}C-PiB in the lung at similar intensity. Another limitation of ^{11}C-PiB-PET is its inability to detect amyloid deposition in the peripheral nervous system, similar to previously reported tracers (Table 3). In conclusion, ^{11}C-PiB-PET imaging can be clinically utilised for systemic evaluation of amyloid distribution in AL and ATTRm amyloidosis patients. Quantitative analysis of ^{11}C-PiB-PET is expected to be useful in therapy evaluation and will reveal whether amyloid clearance is correlated with clinical response.

Compliance with Ethical Standards:

Funding: This study was funded by a Grant-in-aid for Scientific Research (C) (23591237 to Y.S) from Japan Society for the Promotion of Science, a grant from the Amyloidosis Research Committee, the Ministry of Health, Labour and Welfare, Japan, and 2015 Global ASPIRE TTR-FAP Competitive Research Grant Award from Pfizer, Inc.

Conflict of Interest: Author N.E declares that he has no conflict of interest. Author N.K declares that he has no conflict of interest. Author K.O declares that he has no conflict of interest. Author T.Y declares that he has no conflict of interest. Author M.Y declares that he has no conflict of interest. Author Y.S declares that he has no conflict of interest.

Ethical approval: All procedures performed in studies involving human participants were in accordance with the ethical standards of the institutional and/or national research committee

and with the 1964 Helsinki declaration and its later amendments or comparable ethical standards.

Informed consent: Informed consent was obtained from all individual participants included in the study.

References

1. Nordberg A, Carter SF, Rinne J, Drzezga A, Brooks DJ, Vandenberghe R, et al. A European multicentre PET study of fibrillar amyloid in Alzheimer's disease. European journal of nuclear medicine and molecular imaging. 2013;40:104-14. doi:10.1007/s00259-012-2237-2.

2. Johnson KA, Gregas M, Becker JA, Kinnecom C, Salat DH, Moran EK, et al. Imaging of amyloid burden and distribution in cerebral amyloid angiopathy. Annals of neurology. 2007;62:229-34. doi:10.1002/ana.21164.

3. LeVine H, 3rd. Quantification of beta-sheet amyloid fibril structures with thioflavin T. Methods in enzymology. 1999;309:274-84.

4. Antoni G, Lubberink M, Estrada S, Axelsson J, Carlson K, Lindsjo L, et al. In vivo visualization of amyloid deposits in the heart with 11C-PIB and PET. Journal of nuclear medicine : official publication, Society of Nuclear Medicine. 2013;54:213-20. doi:10.2967/jnumed.111.102053.

5. Hellstrom-Lindahl E, Westermark P, Antoni G, Estrada S. In vitro binding of [(3)H]PIB to human amyloid deposits of different types. Amyloid : the international journal of experimental and clinical investigation : the official journal of the International Society of Amyloidosis. 2014;21:21-7. doi:10.3109/13506129.2013.860895.

6. Sekijima Y, Yazaki M, Oguchi K, Ezawa N, Yoshinaga T, Yamada M, et al. Cerebral amyloid angiopathy in posttransplant patients with hereditary ATTR amyloidosis. Neurology. 2016;87:773-81. doi:10.1212/wnl.0000000000003001.

7. Gertz MA, Comenzo R, Falk RH, Fermand JP, Hazenberg BP, Hawkins PN, et al.

Definition of organ involvement and treatment response in immunoglobulin light chain amyloidosis (AL): a consensus opinion from the 10th International Symposium on Amyloid and Amyloidosis, Tours, France, 18-22 April 2004. American journal of hematology. 2005;79:319-28. doi:10.1002/ajh.20381.

8. Sekijima Y, Uchiyama S, Tojo K, Sano K, Shimizu Y, Imaeda T, et al. High prevalence of wild-type transthyretin deposition in patients with idiopathic carpal tunnel syndrome: a common cause of carpal tunnel syndrome in the elderly. Human pathology. 2011;42:1785-91. doi:10.1016/j.humpath.2011.03.004.

9. Scheinin NM, Tolvanen TK, Wilson IA, Arponen EM, Nagren KA, Rinne JO. Biodistribution and radiation dosimetry of the amyloid imaging agent 11C-PIB in humans. Journal of nuclear medicine : official publication, Society of Nuclear Medicine. 2007;48:128-33.

10. Hawkins PN, Lavender JP, Pepys MB. Evaluation of systemic amyloidosis by scintigraphy with 123I-labeled serum amyloid P component. The New England journal of medicine. 1990;323:508-13. doi:10.1056/nejm199008233230803.

11. Rydh A, Suhr O, Hietala SO, Ahlstrom KR, Pepys MB, Hawkins PN. Serum amyloid P component scintigraphy in familial amyloid polyneuropathy: regression of visceral amyloid following liver transplantation. European journal of nuclear medicine. 1998;25:709-13.

12. Nelson SR, Hawkins PN, Richardson S, Lavender JP, Sethi D, Gower PE, et al. Imaging of haemodialysis-associated amyloidosis with 123I-serum amyloid P component. Lancet (London, England). 1991;338:335-9.

13. Rowczenio D, Dogan A, Theis JD, Vrana JA, Lachmann HJ, Wechalekar AD, et al.

Amyloidogenicity and clinical phenotype associated with five novel mutations in apolipoprotein A-I. The American journal of pathology. 2011;179:1978-87. doi:10.1016/j.ajpath.2011.06.024.

14. Hutt DF, Gilbertson J, Quigley AM, Wechalekar AD. (99m)Tc-DPD scintigraphy as a novel imaging modality for identification of skeletal muscle amyloid deposition in light-chain amyloidosis. Amyloid : the international journal of experimental and clinical investigation : the official journal of the International Society of Amyloidosis. 2016;23:134-5. doi:10.3109/13506129.2016.1158160.

15. Puille M, Altland K, Linke RP, Steen-Muller MK, Kiett R, Steiner D, et al. 99mTc-DPD scintigraphy in transthyretin-related familial amyloidotic polyneuropathy. European journal of nuclear medicine and molecular imaging. 2002;29:376-9.

16. Quarta CC, Obici L, Guidalotti PL, Pieroni M, Longhi S, Perlini S, et al. High 99mTc-DPD myocardial uptake in a patient with apolipoprotein AI-related amyloidotic cardiomyopathy. Amyloid : the international journal of experimental and clinical investigation : the official journal of the International Society of Amyloidosis. 2013;20:48-51. doi:10.3109/13506129.2012.746938.

17. Rao BK, Padmalatha C, Au Buchon J, Lieberman LM. Hepatic and splenic scintigraphy in idiopathic systemic amyloidosis. European journal of nuclear medicine. 1981;6:143-6.

18. Janssen S, Piers DA, van Rijswijk MH, Meijer S, Mandema E. Soft-tissue uptake of 99mTc-diphosphonate and 99mTc-pyrophosphate in amyloidosis. European journal of nuclear medicine. 1990;16:663-70.

19. Bokhari S, Castano A, Pozniakoff T, Deslisle S, Latif F, Maurer MS. (99m)Tc-pyrophosphate scintigraphy for differentiating light-chain cardiac amyloidosis from the transthyretin-related familial and senile cardiac amyloidoses. Circulation Cardiovascular imaging. 2013;6:195-201. doi:10.1161/circimaging.112.000132.

20. Nakagawa M, Sekijima Y, Yazaki M, Tojo K, Yoshinaga T, Doden T, et al. Carpal tunnel syndrome: a common initial symptom of systemic wild-type ATTR (ATTRwt) amyloidosis. Amyloid : the international journal of experimental and clinical investigation : the official journal of the International Society of Amyloidosis. 2016;23:58-63. doi:10.3109/13506129.2015.1135792.

21. Dorbala S, Vangala D, Semer J, Strader C, Bruyere JR, Jr., Di Carli MF, et al. Imaging cardiac amyloidosis: a pilot study using (1)(8)F-florbetapir positron emission tomography. European journal of nuclear medicine and molecular imaging. 2014;41:1652-62. doi:10.1007/s00259-014-2787-6.

22. Osborne DR, Acuff SN, Stuckey A, Wall JS. A Routine PET/CT Protocol with Streamlined Calculations for Assessing Cardiac Amyloidosis Using (18)F-Florbetapir. Frontiers in cardiovascular medicine. 2015;2:23. doi:10.3389/fcvm.2015.00023.

23. Broski SM, Spinner RJ, Howe BM, Dispenzieri A, Johnson GB. 18F-Florbetapir and 18F-FDG PET/CT in Systemic Immunoglobulin Light Chain Amyloidosis Involving the Peripheral Nerves. Clinical nuclear medicine. 2016;41:e115-7. doi:10.1097/rlu.0000000000000947.

24. Garcia-Gonzalez P, Sanchez-Jurado R, Cozar-Santiago MP, Ferrando-Beltran M, Perez-Rodriguez PL, Ferrer-Rebolleda J. Laryngeal and cardiac amyloidosis diagnosed by

18F-Florbetapir PET/CT. Revista espanola de medicina nuclear e imagen molecular. 2017;36:135-6. doi:10.1016/j.remn.2016.03.006.

25. Leung N, Ramirez-Alvarado M, Nasr SH, Kemp BJ, Johnson GB. Detection of ALECT2 amyloidosis by positron emission tomography-computed tomography imaging with florbetapir. British journal of haematology. 2017;177:12. doi:10.1111/bjh.14519.

26. D'Estanque E, Chambert B, Moranne O, Kotzki PO, Boudousq V. 18F-Florbetaben: A New Tool for Amyloidosis Staging? Clinical nuclear medicine. 2017;42:50-3. doi:10.1097/rlu.0000000000001434.

27. Aprile C, Marinone G, Saponaro R, Bonino C, Merlini G. Cardiac and pleuropulmonary AL amyloid imaging with technetium-99m labelled aprotinin. European journal of nuclear medicine. 1995;22:1393-401.

28. Schaadt BK, Hendel HW, Gimsing P, Jonsson V, Pedersen H, Hesse B. 99mTc-aprotinin scintigraphy in amyloidosis. Journal of nuclear medicine : official publication, Society of Nuclear Medicine. 2003;44:177-83.

29. Hawkins PN, Pepys MB. Imaging amyloidosis with radiolabelled SAP. European journal of nuclear medicine. 1995;22:595-9.

30. Bokhari S, Shahzad R, Castano A, Maurer MS. Nuclear imaging modalities for cardiac amyloidosis. Journal of nuclear cardiology : official publication of the American Society of Nuclear Cardiology. 2014;21:175-84. doi:10.1007/s12350-013-9803-2.

31. Ohyama T, Shimokama T, Yoshikawa Y, Watanabe T. Splenic amyloidosis: correlations between chemical types of amyloid protein and morphological features. Modern pathology : an official journal of the United States and Canadian Academy of Pathology, Inc.

1990;3:419-22.

32. Martins AC, Rosa AM, Costa E, Tavares C, Quadrado MJ, Murta JN. Ocular Manifestations and Therapeutic Options in Patients with Familial Amyloid Polyneuropathy: A Systematic Review. BioMed research international. 2015;2015:282405. doi:10.1155/2015/282405.

33. Hachulla E, Janin A, Flipo RM, Saile R, Facon T, Bataille D, et al. Labial salivary gland biopsy is a reliable test for the diagnosis of primary and secondary amyloidosis. A prospective clinical and immunohistologic study in 59 patients. Arthritis and rheumatism. 1993;36:691-7.

34. de Paula Eduardo F, de Mello Bezinelli L, de Carvalho DL, Della-Guardia B, de Almeida MD, Marins LV, et al. Minor salivary gland biopsy for the diagnosis of familial amyloid polyneuropathy. Neurological sciences : official journal of the Italian Neurological Society and of the Italian Society of Clinical Neurophysiology. 2017;38:311-8. doi:10.1007/s10072-016-2760-1.

35. Villa F, Dionigi G, Tanda ML, Rovera F, Boni L. Amyloid goiter. International journal of surgery (London, England). 2008;6 Suppl 1:S16-8. doi:10.1016/j.ijsu.2008.12.025.

36. Matsuda M, Gono T, Shimojima Y, Yoshida T, Katoh N, Hoshii Y, et al. AL amyloidosis manifesting as systemic lymphadenopathy. Amyloid : the international journal of experimental and clinical investigation : the official journal of the International Society of Amyloidosis. 2008;15:117-24. doi:10.1080/13506120802006047.

37. Kyle RA, Gertz MA. Primary systemic amyloidosis: clinical and laboratory features in 474 cases. Seminars in hematology. 1995;32:45-59.

38. Matsuda M, Katoh N, Ikeda S. Clinical manifestations at diagnosis in Japanese patients with systemic AL amyloidosis: a retrospective study of 202 cases with a special attention to uncommon symptoms. Internal medicine (Tokyo, Japan). 2014;53:403-12.

Figure legends

Fig. 1. Representative maximum intensity projection (MIP) images of whole-body ^{11}C-PiB-PET. Anterior views (**a** – **c**) and lateral views (**d** – **f**) of MIP images are shown—**a** and **d**: healthy control (subject 16, Table 1); **b** and **e**: AL amyloidosis (patient 1, Table 1); **c** and **f**: ATTRm amyloidosis (patient 12, Table 1). The urinary tract and enterohepatic circulatory system were positively delineated in all participants due to the physiological clearance pathway of ^{11}C-PiB. Abnormal tracer uptake in the heart, spleen, extraocular muscles, parotid gland, tongue, nuchal muscles, submandibular gland and thyroid gland were detectable in the AL patient (**b** and **e**). The lower right lung collapsed due to pleural effusion is illustrated with increased density (**b** and **e**). Abnormal tracer uptake in the heart, scalp, lachrymal gland, parotid gland, nasal mucosa, pharynx, tongue, submandibular gland, sublingual gland, thyroid gland and brain were detected in the ATTRm patient (**c** and **e**).

Fig. 2. Representative transaxial PET images and fused PET/CT images. **A**: healthy control (subject 16, Table 1). **B**: AL amyloidosis (**Ba** – **h** and **j**, patient 1, Table 1; **Bi**, patient 4, Table 1). **C**: ATTRm amyloidosis (**Ca** – **b**, patient 9, Table 1; **Cc** – **j**, patient 12, Table 1). Increased ^{11}C-PiB retention in the brain (**Ca**), scalp (**Ca**, **b**), lachrymal gland (**Cc**), extraocular muscles (**Bc**), nuchal muscles (**Bc** – **g**), parotid gland (**Ad** – **e**, **Bd** – **e**, **Cd** – **e**), nasal mucosa (**Cd**), pharynx (**Cd** – **f**), tongue (**Be** and **Ce**), submandibular gland (**Bf** and **Cf**), sublingual gland (**Cf**), thyroid gland (**Bg** and **Cg**), heart (**Bh** and **Ch**), lung (**Ah**, **Bh**, **Ch**), liver (**Ai** – **j**, **Bi** – **j**, **Ci** – **j**), gastric wall and spleen (**Bi** and **Ci**) and small intestine and kidneys (**Aj**, **Bj**, **Cj**) are

shown.

Fig. 3. Correlations between ^{11}C-PiB-PET images and histopathological findings. **a** – **d**: Gastric images of AL amyloidosis patient (patient 4, Table 1). Transaxial fused PET/CT image of the stomach (**a**) showed mild ^{11}C-PiB tracer uptake in the gastric wall (arrowheads). Congo red staining of biopsied gastric mucosa specimen showed considerable amyloid deposition in muscularis mucosae, submucosal connective tissue and lamina propria (**b**; **c**, polarised view), and all of these deposits were specifically immunolabelled with anti-Aλ antibody (**d**). Scale bars in **b** – **d** are 400 μm. **e** – **h**: Cardiac images of ATTRm amyloidosis patient (patient 14, Table 1). Transaxial fused PET/CT image of the heart (**e**) showed mild ^{11}C-PiB tracer uptake in the left ventricular wall and intraventricular septum (arrowheads) and in the anterior wall of right ventricle (arrow). Congo red staining of biopsied endomyocardial specimen showed moderate amyloid deposition in interstitial tissue around cardiomyocytes (**f**; **g**, polarised view). All of these deposits were specifically immunolabelled with anti-TTR antibody (**h**). Scale bars in **f** – **h** are 100 μm.

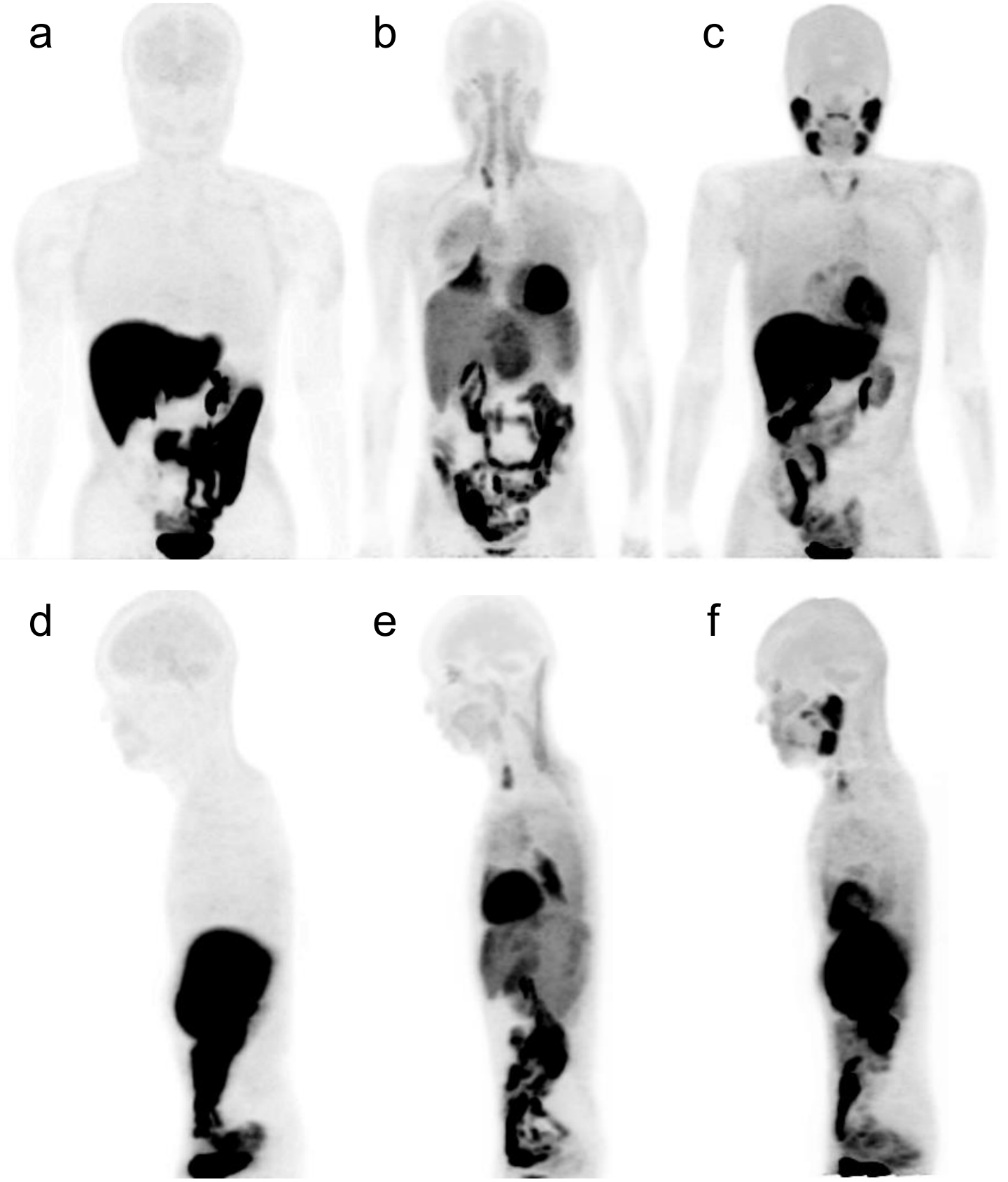
a
b
c
d
e
f

A. Healthy control

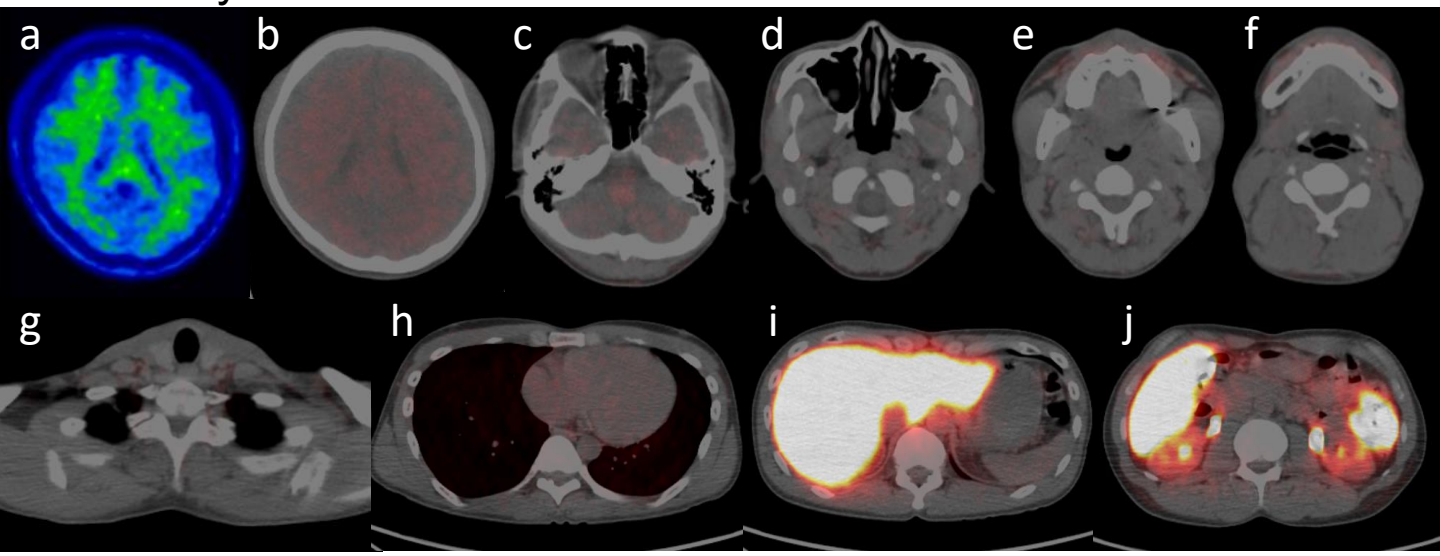

B. AL amyloidosis

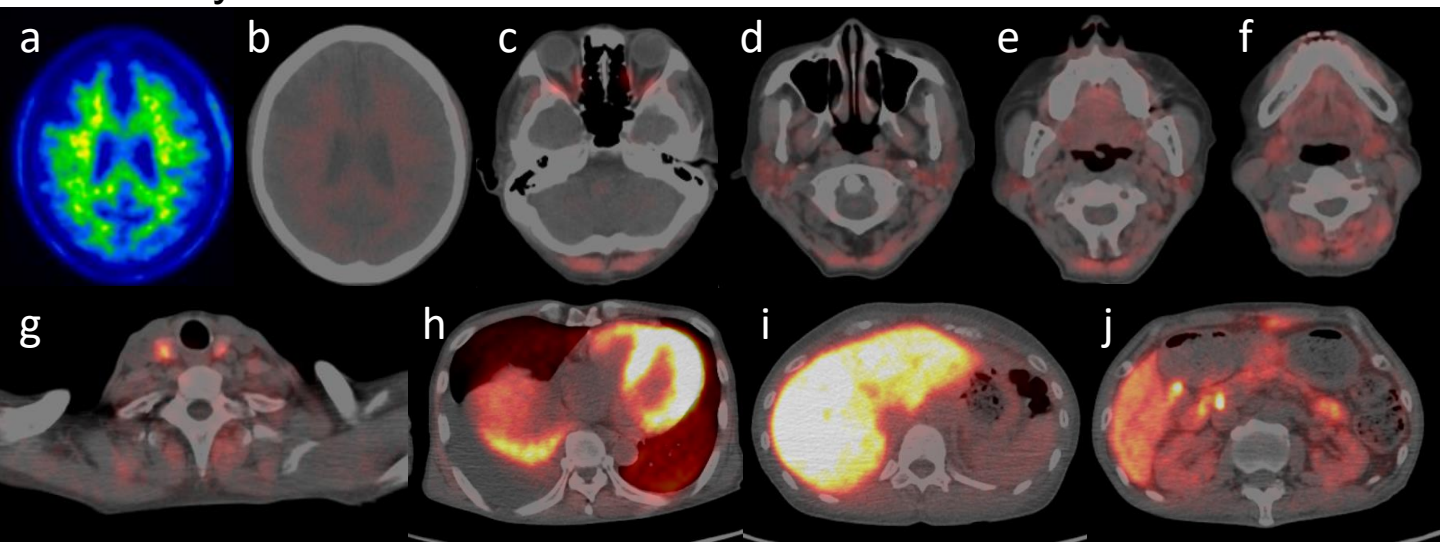

C. ATTRm amyloidosis

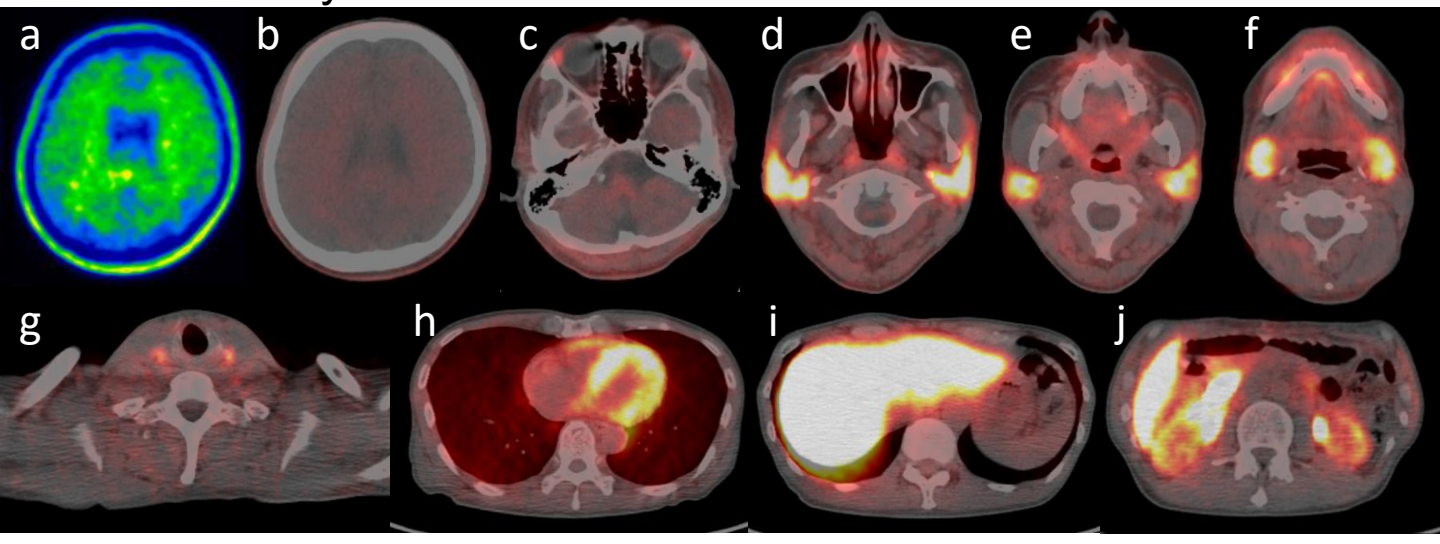

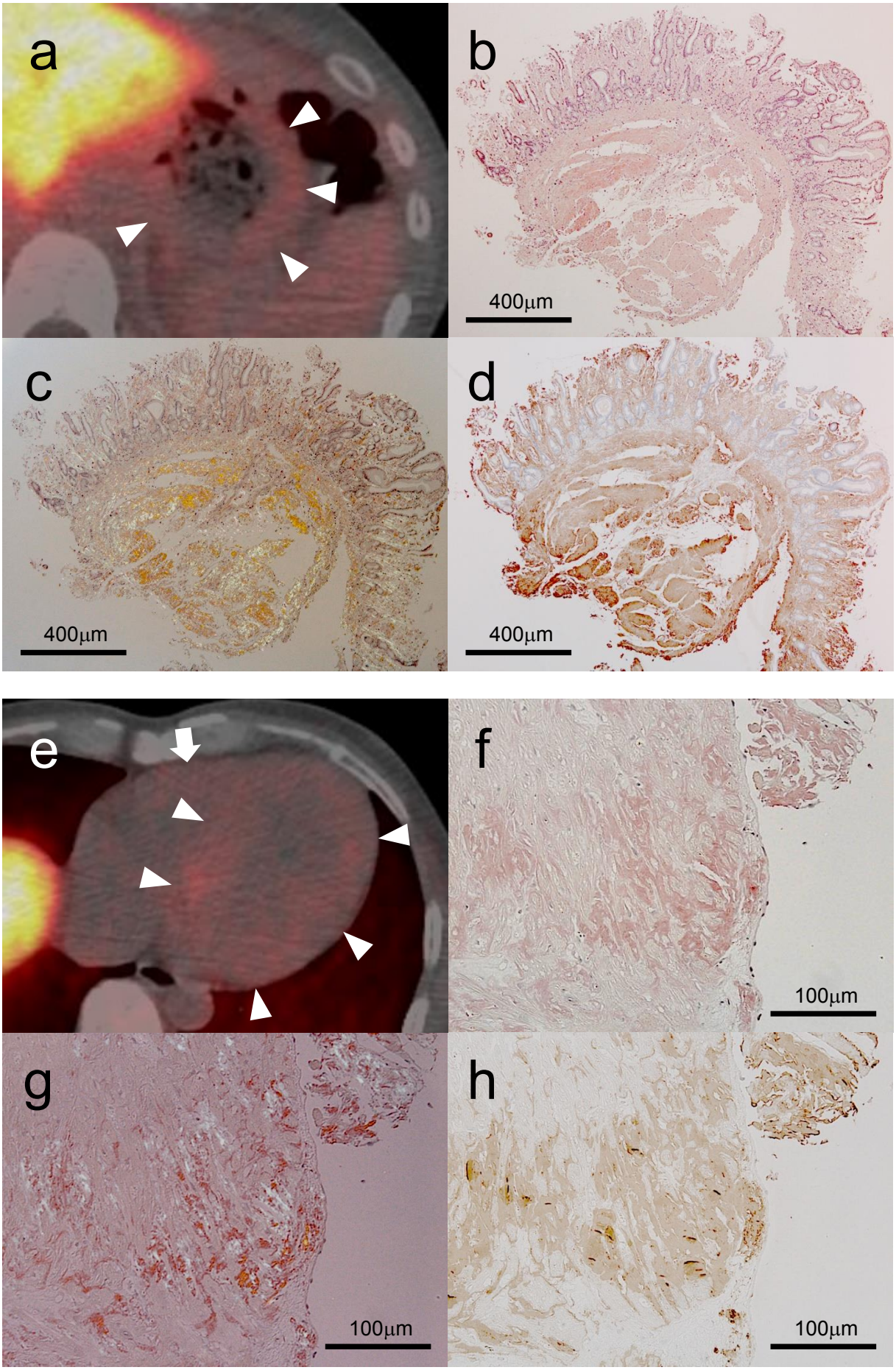
a
b
400μm
c
400μm
d
400μm
e
f
100μm
g
100μm
h
100μm

Table 1. Clinical background, organ involvement, and ^{11}C-PiB tracer uptake

No.	Diagnosis	Age	Sex	Treatment history		Organ involvement and PiB tracer uptake																	
									Glandular tissues						CNS	PNS		Soft tissues					
						Ht	St	Sp	LG	PG	SmG	SlG	TG	LN	Brain	SmN	AN	Sc	EM	Na	Ph	Tg	NM
1	Systemic AL amyloidosis	56	M	Chemotherapy	Organ involvement	+	+						(+)			+	+					+	
					Tracer uptake	+++	+	++		+	+		+++						+			+	++
2	Systemic AL amyloidosis	71	M	None	Organ involvement	+							(+)										
					Tracer uptake	++				+	+											+	++
3	Systemic AL amyloidosis	82	F	None	Organ involvement	+							(+)									+	(+)
					Tracer uptake	+		+						++								+	+
4	Systemic AL amyloidosis	52	F	None	Organ involvement	+	+				(+)		(+)										
					Tracer uptake	+	+	+			+		+						+			+	+
5	Systemic AL amyloidosis	69	F	None	Organ involvement	+																	
					Tracer uptake	++	+			+												+	
6	Systemic AL amyloidosis	59	M	None	Organ involvement	+							(+)										
					Tracer uptake	+++		++		+			+									+	++
7	Systemic AL amyloidosis	57	F	None	Organ involvement																		
					Tracer uptake																	+	
8	Hereditary ATTR amyloidosis (V30M)	43	F	LDLT	Organ involvement	+	+						(+)			+	+						
					Tracer uptake	++	+		+													++	
9	Hereditary ATTR amyloidosis (V30M)	45	M	LDLT, Tafamidis	Organ involvement	+	+						(+)			+	+						
					Tracer uptake	++	+		+	++	++		++		+			+		+	++	+	
10	Hereditary ATTR amyloidosis (G47R)	23	F	Tafamidis	Organ involvement	+	+		(+)				(+)			+	+						
					Tracer uptake		+	++	+	+	+		+									+	
11	Hereditary ATTR amyloidosis (V30M)	43	M	LDLT	Organ involvement		+									+	+						
					Tracer uptake	+++	+		+	+++	+++		+++					+		+	++	+	
12	Hereditary ATTR amyloidosis (V30M)	43	M	BDLT	Organ involvement	+										+	+						
					Tracer uptake	+++	+		++	+++	+++	++	+++					+		+	++	+	
13	Hereditary ATTR amyloidosis (V30M)	55	M	BDLT, PM, Tafamidis	Organ involvement	+	+									+	+						
					Tracer uptake	+++	+			++	+		+		+						+	+	
14	Hereditary ATTR amyloidosis (T60A)	58	M	None	Organ involvement	+	+										+						
					Tracer uptake	+	+			+												+	
15	Asymptomatic *TTR* mutation carrier (D18G)	28	F	None	Organ involvement																		
					Tracer uptake																		
16	Healthy control	39	M	None	Organ involvement																		
					Tracer uptake																		
17	Healthy control	38	M	None	Organ involvement																		
					Tracer uptake					+													
18	Healthy control	50	M	None	Organ involvement																		
					Tracer uptake																		

PiB: Pittsburgh compound B, AL amyloidosis: light-chain amyloidosis, ATTR amyloidosis: transthyretin amyloidosis, Ht: heart, St: stomach, Sp: spleen, LG: lachrymal gland, PG: parotid gland, SmG: submandibular gland, SlG: sublingual gland, TG: thyroid gland, LN: lymph node, CNS: central nervous system, PNS: peripheral nervous system, SmN: sensorymotor neuropathy, AN: autonomic neuropathy, Sc: scalp, EM: extraocular muscles, Na: nasal mucosa, Ph: pharynx, Tg: tongue, NM: nuchal muscles, LDLT: living-donor partial liver transplantation, BDLT: brain-dead donor liver transplantation, PM: pacemaker, Tracer uptake grading: +: mild; ++: moderate; +++: intense,

Gray boxes: organ involvements not determined by international consensus criteria [7]; (+): organ-related symptoms without consensus involvement criteria.

Table 2. Organ involvement criteria in this study*

Organ	Criterion for organ involvement
Heart	Mean left ventricular wall thickness > 12 mm, no other cardiac cause
Kidney	24 hour urine protein > 0.5 g/day, predominantly albumin
Liver	Total liver span > 15 cm or alkaline phosphatase > 1.5 times institutional upper limit of normal
Gastrointestinal tract	Direct biopsy verification with symptoms
Lung	Direct biopsy verification with symptoms, Interstitial radiographic pattern
Nerve	Peripheral: clinical; symmetric lower extremity sensorimotor peripheral neuropathy Autonomic: gastric-emptying disorder, pseudo-obstruction, voiding dysfunction not related to direct organ infiltration
Tongue	Tongue enlargement, clinical
Lymph node	Lymphadenopathy

*Determined by international consensus guideline [7]

Table 3. Amyloid imaging techniques for systemic amyloidosis

Tracer	Type of amyloidosis	Advantages	Limitations	Reference
^{123}I-SAP	AL and AA	Amyloid detectable in the spleen, kidneys, adrenals, bone marrow, carpal region, skin, and tongue.	The heart was undetectable. Positive liver scintigrapy was observed even among the patients whose liver function (including ALP) was totally normal.	Hawkins. N Engl J Med 1990 [10]
	ATTRm	Amyloid detectable in the spleen, kidneys, and adrenals.	The heart, GI tract, and nerve were undetectable. Liver scintigraphy was positive in all patients whose hepatic amyloid was histologically confirmed to be absent.	Rydh. Eur J Nucl Med 1998 [11]
	Aβ2M	Amyloid detectable in the affected joints (wrists and knees) and spleen.	Low sensitivity to detect the shoulder and hip joints arthropathy.	Nelson. Lancet 1991 [12]
	AApo-AI	Amyloid detectable in the spleen, kidneys, and liver.	Amyloid deposition were undetectable in the skin, vocal cord, heart, nerves, and testes.	Rowczenio. Am J Pathol 2011 [13]
^{99m}Tc-DPD	AL	Amyloid detectable in the skeletal muscle.	About half of patients with cardiac involvement did not show positive scintigraphy. The other visceral organs showed negative uptake.	Hutt. Amyloid 2016 [14]
	ATTRm	Amyloid detectable in the heart, joints, lower GI tract, thoracic and abdominal wall.	No significant liver or spleen uptake in patient. Physiological positive uptake in the urinary tract (kidney, ureter, and bladder) in patients and controls.	Puille. Eur J Nucl Med 2002 [15]
	AApo-AI	Amyloid detectable in the heart.	Data unknown for hepatic, renal, and neuropathic involvements.	Quarta. Amyloid 2013 [16]
^{99m}Tc-PYP	AL	Amyloid detectable in the spleen, limbs, tongue, and thyroid.	No significant correlationship between cardiac amyloidosis and cardiac uptake. Limited relationship between organ involvement and tracer uptake in the liver, GI tract, and kidneys.	Rao. Eur J Nucl Med 1981 [17] Janssen. Eur J Nucl Med 1990 [18]
	ATTRm and ATTRwt	Cardiac involvement is sensitively detectable.	Capability to detect organ involvement other than the heart is undetermined.	Bokhari. Circ Cardiovasc Imaging 2013 [19] Nakagawa. Amyloid 2016 [20]
^{99m}Tc-MDP	AL and AA	Amyloid detectable in the limbs, tongue, and thyroid.	No significant correlationship between cardiac amyloidosis and cardiac uptake. Limited relationship between organ involvement and tracer uptake in the liver, GI tract, and kidneys.	Janssen. Eur J Nucl Med 1990 [18]
^{18}F-Florbetapir	AL and ATTR	Amyloid detectable in the heart in both AL and ATTR amyloidosis.	Data unknown for the other organs.	Dorbala. Eur J Nucl Med Mol Imaging 2014 [21] Osborne. Front Cardiovasc Med 2015 [22]
	AL	Amyloid detectable in the peripheral nerve and possibly in the muscles.	The number of investigated patients was limited to the one (case report).	Broski. Clin Nucl Med 2016 [23]
	AL	Amyloid detectable in the heart and larynx.	The number of investigated patients was limited to the one (case report).	García-González. Rev Esp Med Nucl Imagen Mol 2017 [24]
	ALECT2	Positive uptake was observeded in the lungs, spleen, adrenal glands, kidneys, and bone marrow.	The number of investigated patients was limited to the one (case report).	Leung. Br J Haematol 2017 [25]
^{18}F-Florbetaben	AL	Positive uptake was observed in the heart, spleen, thyroid, salivary gland, and kidney.	The number of investigated patients was limited to the one (case report).	D'Estanque. Clin Nucl Med 2017 [26]
^{99m}Tc-Aprotinin	AL (and ATTRm)	Amyloid detactable in the heart, pleura, lung, thyroid, pericardium, sternum, tongue, salivary glands, lymph node, oropharynx, larynx, intestines and joints.	The number of investigated patients with ATTRm was very limited. Underdiaphragmatic organs (such as the kidney, liver, spleen) were not evaluable due to the high scattering from the kidneys. Central or peripheral nervous system involvement was undetectable.	Aprile. Eur J Nucl Med 1995 [27] Schaadt. J Nucl Med 2003 [28]
^{11}C-PiB	AL and ATTRm	Good correlationship between clinical and radiological involvement in the heart and stomach. Positive uptake in the tongue, lymph node, spleen, lachrymal gland, salivary glands, thyloid, brain, scalp, extraocular muscles, nasal mucosa, pharynx, nuchal muscles.	Physiological uptake in the lung, urinary tract, and enterohepatic circulation system. Peripheral nervous system involvement was undetectable.	This study

SAP: serum amyloid P, DPD: diphosphono-1,2-propanodicarboxylic acid, PYP: pyrophosphate, MDP: methylene diphosphonate, PiB: Pittsburgh compound B
AL: light-chain amyloidosis, AA: serum amyloid A amyloidosis, ATTRm: hereditary transthyretin amyloidosis, Aβ2M: β2-microglobulin amyloidosis
AApo-AI: apolipoprotein A I amyloidosis, ATTRwt: systemic wild-type transthyretin amyloidosis, ALECT2: leucocyte cell-derived chemotaxin 2 amyloidosis